Exceptionally Bright TeV Emission From the Binary LS I +61° 303

Andy Smith[1], Anna OFdB[2], VERITAS Collaboration[3]

ABSTRACT

The TeV binary system LS I +61° 303 is known for its regular, although not entirely understood, non-thermal emission pattern, which traces the orbital period of the compact object in its 26.5 day orbit around its Be star companion. When active in the TeV regime, the system typically presents elevated emission around apastron passage with flux levels in the 5 – 15 % Crab Nebula range (> 300 GeV). In this article, VERITAS observations of LS I +61° 303 taken in late 2014 are presented, in which bright TeV flares around apastron at flux levels peaking above 30% of the Crab Nebula flux were detected. This is the brightest such activity ever seen in the TeV regime. The strong outbursts have rise and fall times of ~2 days with flux doubling times less than a day. This short acceleration time provides constraints on the nature and efficiency of the accelerating mechanism in the source.

Subject headings:

1. Introduction

The current generation of Imaging Atmospheric Cherenkov Telescopes (IACTs) has opened up the study of high mass X-ray binary star systems which also present TeV emission on various timescales. The class of TeV binaries is quite sparse, consisting of only a handful of sources: LS 5039 (Aharonian et al. 2005b), PSR B1259-63 (Aharonian et al. 2005a), LS I +61° 303 (Albert et al. 2006), HESS J0632+057 (Acciari et al. 2009), and the newest member of the class HESS J1018-589A (Abramowski et al. 2015). Of these, only the compact object of PSR B1259-63 has been firmly identified as a pulsar; there is still a large degree of ambiguity concerning the nature of the compact object within the other systems, and consequently, the fundamental setup which produces the TeV emission along with its characteristic variability on the orbital period timescale.

The orbital periods of these objects vary from several days (LS 5039) to several years (PSR B129-63), and as a result, the various sources may only present short windows during which they can be studied in the TeV regime. Of the TeV binaries, LS I +61° 303 is the only known source in the Northern Hemisphere which has a short enough orbital period (26.5 days) to allow for regular study with TeV instruments. This has made it an excellent target for Northern Hemisphere TeV observatories.

LS I +61° 303, located at a distance of ~2 kpc, is composed of a B0 Ve star and a compact object (Hutchings & Crampton 1981; Casares et al. 2005). The observed radio to TeV emission is variable and modulated with a period of $P \approx 26.5$ days, believed to be associated with the orbital structure of the binary system (Albert et al. 2006; Esposito et al. 2007; Acciari et al. 2008; Abdo et al. 2009; Li et al. 2012; Massi et al. 2015). Radial velocity measurements show the orbit to be elliptical $e = 0.537 \pm 0.034$, with periastron occurring around phase $\phi = 0.275$, apastron at $\phi = 0.775$, superior conjunction at $\phi = 1.081$ and inferior conjunction at $\phi = 0.313$ (Aragona et al. 2009). The periastron distance between the star and the compact object is estimated at 2.84×10^{12} cm (0.19 AU), and the apastron distance at 9.57×10^{12} cm (0.64 AU) (Dubus 2013).

[1]America

[2]Germany

[3]Everywhere

However, the inclination of the system is not exactly known (it is expected to lie in the range 10° – 60°), leading to some uncertainty of the orbital parameters.

In this work, we present the results of the VERITAS campaign on LS I +61° 303 in the Fall of 2014. During this time, VERITAS observed historically bright flares from LS I +61° 303 around apastron, with the source exhibiting flux levels a factor of 2 – 3 times higher than previously seen.

2. Observations

The VERITAS IACT array, located at the base of Mt. Hopkins, AZ (1.3 km a.s.l., 31°40' N, 110°57' W) consists of four 12 m diameter Davies-Cotton design optical telescopes. VERITAS is sensitive from 85 GeV to 30 TeV, and has the ability to detect a 1 % Crab Nebula source in approximately 25 hours[1]. For a full description of the hardware components and analysis methods utilized by VERITAS, see Holder et al. (2008); Kieda, D., for the VERITAS Collaboration (2013); Acciari et al. (2008), and references therein.

In the 2014 season, VERITAS observations of LS I +61° 303 were taken from October 16 (MJD 56946) to December 12 (MJD 57003), obtaining a total of 24.7 hours of quality selected livetime. These observations covered three separate orbital periods of LS I +61° 303, sampling the orbital regions of $\phi = 0.5 - 0.2$ (see Figure 1 and Table 1). Over the entire set of observations, a total of 449 excess events above background were detected, equivalent to a significance of 21σ calculated using Equation 17 of Li & Ma (1983).

During the first orbit observed (in October), the source presented the largest of its flares (hereafter "F1"), beginning on 2014 October 17 (MJD 56947, $\phi = 0.55$) with emission reaching a peak of $31.9 \pm 3.4 \times 10^{-12}$ photons cm^{-2} s^{-1} (>300 GeV) on October 18 (MJD 56948). This flare peaked at approximately 30% of the Crab Nebula flux in the same energy range, representing the largest flux ever detected from the source. Unfortunately, observations were limited by poor weather conditions for two nights following this peak and only recommenced on October 20 (MJD 56950),

[1]http://veritas.sao.arizona.edu/about-veritas-mainmenu-81/veritas-specifications-mainmenu-111

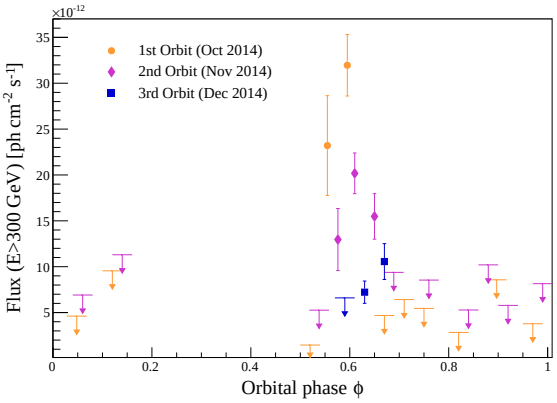

Fig. 1.— Light curve of LS I +61° 303 during the 2014 observation season in nightly bins. The data is shown in the different orbits observed, with the first orbit (October) shown with orange circles, the second orbit shown with purple diamonds, and the third orbit shown with blue squares. Flux upper limits at the 99% confidence level are shown for points with $< 3\,\sigma$ significance and are represented by arrows.

by which time the source had already quietened down. During the November observations (second orbital passage), VERITAS detected another period of high activity ("F2") from the source at similar orbital phases ($\phi = 0.5 - 0.6$) with peak emission of $20.2 \pm 2.2 \times 10^{-12}$ photons cm^{-2} s^{-1} (>300 GeV) on November 14 (MJD 56975).

The rise and fall times of the flares was determined by fitting a Gaussian on top of a constant baseline to the light curve of each orbit, and also by comparing the flux on the peak night of each flare to the flux levels on different nights before and after the peak. Both F1 and F2 were found to have rise/fall times of ~2 days. The rapid increase in flux at the onset of F1 implies flux doubling timescales of less than a day. Similar to the findings of Aliu et al. (2013), a hint of nightly variability at a significance level of ~$3.5\,\sigma$ was found in F1.

Follow-up observations conducted by VERITAS during the next month (2014 December 10 – 12) covered the orbital phases of $\phi = 0.59 - 0.67$ and detected the source at a lower flux level, reaching only $7.2 \pm 1.2 \times 10^{-12}$ photons cm^{-2} s^{-1} (>300 GeV) around the orbital phase at which

TABLE 1
VERITAS OBSERVATIONS OF LS I +61° 303 IN 2014

Date observed [MJD]	Orbital phase (ϕ)	Flux($> 300\,\mathrm{GeV}$) [$\times 10^{-11}$ cm^{-2} s^{-1}]
56946.3	0.52	<0.15
56947.3	0.55	2.32 ± 0.54
56948.3	0.60	3.20 ± 0.34
56950.0	0.67	<0.47
56951.0	0.71	<0.64
56952.0	0.75	<0.55
56954.0	0.82	<0.28
56956.0	0.90	<0.86
56958.0	0.97	<0.38
56960.0	0.05	<0.46
56962.0	0.12	<0.96
56973.0	0.54	<0.53
56974.0	0.58	1.30 ± 0.34
56975.0	0.61	2.02 ± 0.22
56976.0	0.65	1.55 ± 0.25
56977.0	0.69	<0.94
56979.0	0.76	<0.85
56981.0	0.84	<0.53
56982.0	0.88	<1.02
56983.0	0.92	<0.58
56985.0	0.99	<0.82
56987.0	0.06	<0.69
56989.0	0.14	<1.13
57001.0	0.59	<0.66
57002.0	0.63	0.72 ± 0.12
57003.0	0.67	1.06 ± 0.20

the flares were detected in the previous orbits. The observations during this month exclude the type of peaked flaring behavior seen at the same phase range in the previous two orbital cycles, perhaps indicating some orbit-to-orbit variations in the source.

During the 2014 observing season, the average differential energy spectrum of LS I +61° 303 was consistent with past observations, i.e., the emission in the $0.3 - 20\,\mathrm{TeV}$ range is well fit by a power-law described by $(1.70 \pm 0.69_{\mathrm{stat}}) \times 10^{-12} \cdot \left(\frac{E}{1\mathrm{TeV}}\right)^{-2.35\pm0.32_{\mathrm{stat}}}$ cm^{-2} s^{-1} TeV^{-1}. Differential energy spectra were also extracted from F1 (October 17-18) and F2 (November 13-15) and show a similar spectral shape, albeit with a higher normalization constant. The spectrum of F1 is described by $(8.6 \pm 1.0_{\mathrm{stat}}) \times 10^{-12} \cdot \left(\frac{E}{1\mathrm{TeV}}\right)^{-2.24\pm0.12_{\mathrm{stat}}}$ cm^{-2} s^{-1} TeV^{-1}, and the spectrum of F2 is described by $(4.8 \pm 0.4_{\mathrm{stat}}) \times 10^{-12} \cdot \left(\frac{E}{1\mathrm{TeV}}\right)^{-2.36\pm0.12_{\mathrm{stat}}}$ cm^{-2} s^{-1} TeV^{-1}. The average and flare spectra are shown in Figure 2 along with previous spectral measurements for comparison. The highest energy gamma-ray observed during this observations was detected during F1 with an energy of ~10 TeV.

During these observations, the source was also monitored by *Fermi*-LAT (0.1 – 300 GeV), *Swift*-XRT (0.2 – 10 keV), and both the RATAN and AMI radio instruments (4/6 – 15 GHz). In addition, H-alpha monitoring of the system took place with the Ritter Observatory in Toledo, Ohio (USA). After the second flare (November) was detected by VERITAS, an ATel (Holder 2015) was released, notifying the astronomical community of the historic flux levels and triggering more intense observations with the existing multiwavelength partners, as well as additional observations with the MAGIC TeV observatory. The results of this campaign are under analysis and will be presented in an upcoming publication.

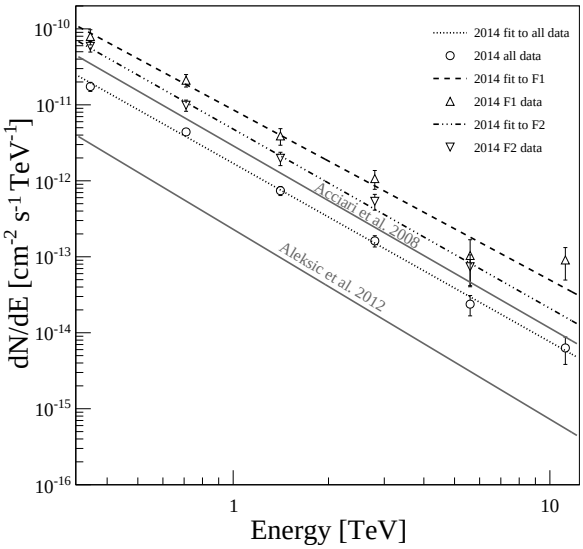

Fig. 2.— Average and flare differential energy spectra of LS I +61° 303 from the VERITAS 2014 observations, shown in comparison with the average spectra from Acciari et al. (2008) and Aleksic et al. (2012).

3. Discussion and Conclusion

The nature of the compact object in LS I +61° 303 is not firmly established, and emission mechanisms proposed for the system cover both a microquasar scenario, in which non-thermal process occur in the jet of an accreting compact object (Massi et al. 2001; Massi & Jaron 2013; Massi et al. 2015), and a pulsar wind shock scenario, in which particle acceleration is the result of the interaction between the stellar and the pulsar winds (Dhawan et al. 2006). In a leptonic scenario, the TeV emission is the result of inverse-Compton (IC) scattering. Khangulyan et al. (2008) provide the means to calculate model-independent limits on the magnetic field strength and the efficiency of the accelerator within an IC scenario. It is assumed that the gamma rays are produced in the system by the IC scattering of TeV electrons on stellar photons. Given the temperature $T = 2.25 \times 10^4\,\mathrm{K}$ (Dubus 2013) of the Be star in LS I +61° 303, the average energy of the stellar photons is $3kT \approx 6\,\mathrm{eV}$, and the IC scattering will take place in the deep Klein–Nishina regime in which all of the electron energy is transferred to the scattered photons. Thus, the presence of ~10 TeV photons requires ~10 TeV electrons in the emitter and the acceleration time must be less than the cooling time. The acceleration timescale of the electrons can be expressed as

$$t_{\mathrm{acc}} = \eta_{\mathrm{acc}} r_{\mathrm{L}} c^{-1} \approx 0.1 \eta_{\mathrm{acc}} E_{\mathrm{TeV}} B_{\mathrm{G}}^{-1}\,\mathrm{s}, \quad (1)$$

where $r_{\rm L}$ is the Larmor radius of the electron, $E_{\rm TeV}$ is the energy of the electron in units of TeV, $B_{\rm G}$ is the magnetic field strength in units of Gauss, and $\eta_{\rm acc} > 1$ is a parameter describing the efficiency of the accelerator (in general $\eta_{\rm acc} \gg 1$). The characteristic cooling time of electrons in the Klein–Nishina regime is given by

$$t_{\rm KN} \approx 10^3 d_{13}^2 E_{\rm TeV}^{0.7}\,{\rm s}, \quad (2)$$

where d_{13} is the distance between the emitter and the optical star in units of 10^{13} cm, and the synchrotron cooling time is

$$t_{\rm sy} \approx 4 \times 10^2 B_{\rm G}^{-2} E_{\rm TeV}^{-1}\,{\rm s}. \quad (3)$$

Hard gamma-ray spectral indices (from -2 to -2.5) require that $t_{\rm KN} < t_{\rm sy}$, as IC losses in the Klein–Nishina regime allow for the electron spectra harder than -2 necessary to produce such gamma-ray indices. Thus, the magnetic field in the emitter is constrained by the relation

$$B < 0.6 d_{13}^{-1} E_{\rm TeV}^{-0.85}\ {\rm G}. \quad (4)$$

This gives values of $B \lesssim 0.3$ G at periastron and $B \lesssim 0.1$ G at apastron, assuming that the emitter is located close to the compact object.

As the cooling time is dominated by $t_{\rm KN}$, the requirement that the acceleration time is less than the cooling time yields the relation $t_{\rm acc} < t_{\rm KN}$ which gives

$$B > 10^{-4} d_{13}^{-2} E_{\rm TeV}^{0.3} \eta_{\rm acc}\ {\rm G}. \quad (5)$$

This gives values of $B \gtrsim 0.125 \eta_{\rm acc}$ G at periastron and $B \gtrsim 0.011 \eta_{\rm acc}$ G at apastron, if the emitter is close to the compact object. Using the lower and upper limits on the magentic field strength, an upper limit can be placed on the acceleration efficieny of $\eta_{\rm acc} \lesssim 120$ at periastron and $\eta_{\rm acc} \lesssim 454$ at apastron.

Figure 3 shows the acceleration time $t_{\rm acc}$ as a function of the magnetic field strength B for different values of the accelerator efficiency $\eta_{\rm acc}$, assuming an electron energy of 10 TeV. The upper limits on the magnetic field strength at periastron and apastron, which are independent of $\eta_{\rm acc}$, are marked. Two areas of the plot are shaded to indicate the allowed regions of the parameter space, corresponding to $t_{\rm acc} < 1$ day, $B < 0.3$ G, and $\eta_{\rm acc} < 120$ at periastron, and $t_{\rm acc} < 1$ day, $B < 0.1$ G, and $\eta_{\rm acc} < 454$ at apastron.

The constraints are strongly dependent on the location of the emitter, which has been assumed to be conincident with the compact object in order to derive these limits. A more detailed discussion of the relationships can be found in Khangulyan et al. (2008).

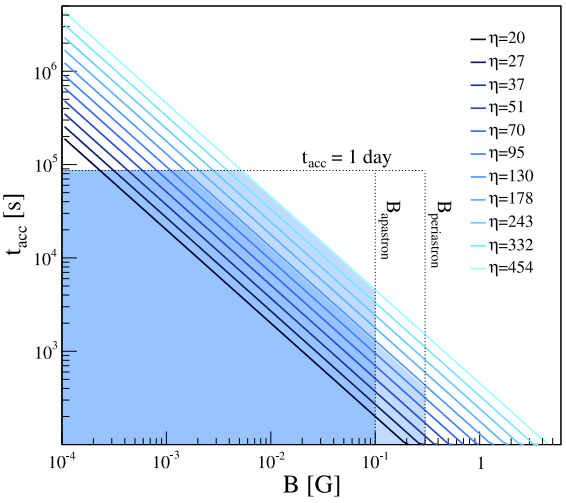

Fig. 3.— Acceleration time $t_{\rm acc}$ as a function of the magnetic field strength B for different values of the accelerator efficiency $\eta_{\rm acc}$, assuming an electron energy of 10 TeV. The horizontal dotted line marks an acceleration time of one day, the maximum acceleration time of the 10 TeV electrons in the system from these observations. The vertical lines marked $B_{\rm apastron}$ and $B_{\rm periastron}$ mark the upper limits on the magnetic field strength at apastron and periastron respectively (these limits are independent of $\eta_{\rm acc}$). The shaded regions show the allowed regions of the parameter space for the system at apastron and periastron.

Paredes-Fortuny, X. et al. (2015) present a general pulsar wind shock scenario with an inhomogeneous stellar wind in which the Be star disc is disrupted and fragments, and these fragments fall into the shock region, pushing it closer to the pulsar. The reduction in size of the pulsar wind termination shock could allow for increased acceleration efficiency on the timescale of a few hours, depending on the size and density of the disc fragments. Such a scenario could account for the exceptionally bright TeV flares and orbit-to-orbit variations seen in LS I +61° 303.

This research is supported by grants from the U.S. Department of Energy Office of Science, the U.S. National Science Foundation and the Smithsonian Institution, by NSERC in Canada, by Science Foundation Ireland (SFI 10/RFP/AST2748) and by STFC in the U.K. We acknowledge the excellent work of the technical support staff at the Fred Lawrence Whipple Observatory and at the collaborating institutions in the construction and operation of the instrument. The VERITAS Collaboration is grateful to Trevor Weekes for his seminal contributions and leadership in the field of VHE gamma-ray astrophysics, which made this study possible. A. O'FdB acknowledges support through the Young Investigators Program of the Helmholtz Association.

REFERENCES

Abdo, A., et al. 2009, ApJ, 701, L123

Abramowski, A., Aharonian, F., Ait Benkhali, F., et al. 2015, ArXiv e-prints, arXiv:1503.02711

Acciari, V., et al. 2008, ApJ, 679, 1427

Acciari, V. A., Aliu, E., Arlen, T., et al. 2009, ApJ, 698, L94

Aharonian, F., Akhperjanian, A. G., Aye, K.-M., et al. 2005a, A&A, 442, 1

—. 2005b, Science, 309, 746

Albert, J., et al. 2006, Science, 312, 1771

Aleksic, J., et al. 2012, ApJ, 746, 80

Aliu, E., Archambault, S., Behera, B., et al. 2013, ApJ, 779, 88

Aragona, C., et al. 2009, ApJ, 698, 514

Casares, J., et al. 2005, MNRAS, 360, 1105

Dhawan, V., et al. 2006, in Proc. of Microquasars and Beyond:From Binaries to Galaxies, in Proceedings of Science, Como, IT, ed. T. Belloni, p.52

Dubus, G. 2013, A&A Rev., 21, 64

Esposito, P., Caraveo, P. A., Pellizzoni, A., et al. 2007, A&A, 474, 575

Holder, J. 2015, The Astronomer's Telegram, 6785

Holder, J., et al. 2008, American Institute of Physics Conference Series, 1085, 657

Hutchings, J., & Crampton, D. 1981, PASP, 93, 486

Khangulyan, D., Aharonian, F., & Bosch-Ramon, V. 2008, MNRAS, 383, 467

Kieda, D., for the VERITAS Collaboration. 2013, in Proceedings of the 33rd International Cosmic Ray Conference (ICRC2013)

Li, J., et al. 2012, ApJ, 744, L13

Li, T.-P., & Ma, Y.-Q. 1983, The Astrophysical Journal, 272, 317

Massi, M., & Jaron, F. 2013, A&A, 554, A105

Massi, M., Jaron, F., & Hovatta, T. 2015, A&A, 575, L9

Massi, M., et al. 2001, A&A, 376, 217

Paredes-Fortuny, X., Bosch-Ramon, V., Perucho, M., & Rib, M. 2015, A&A, 574, A77

This 2-column preprint was prepared with the AAS LaTeX macros v5.2.